Journal of Structural Engineering & Applied Mechanics (2022) 5(4):249-263
DOI 10.31462/jseam.2022.04249263

RESEARCH ARTICLE

The behavior of the historical Çobandede bridge under flood load

İrfan Kocaman*, Muhammet Yılmaz, Fatih Tosunoğlu, İlker Kazaz

Erzurum Technical University, Department of Civil Engineering, Erzurum, Türkiye

Article History

Received 28 September 2022
Accepted 25 December 2022

Keywords

Çobandede bridge
Historical bridge behavior
Flood load
Annual maximum flow
Probability distribution

Abstract

Determination of the structural behavior of historical monuments under different loading types is a crucial task for the preservation and conservation of these structures for transferring to future generations. In this study, the behavior of 800 years old historical Erzurum Çobandede bridge under flood load is investigated. To determine the flood load subjected to the bridge, the best probability distribution model was selected for the observed data obtained from flow gauging stations in the nearby Kağızman Basin and then flood data at different return periods were estimated with this model. The behavior of the bridge under maximum flood load is determined. It is specified that the bridge will not suffer serious damage under the possible maximum flood load in different return periods.

1. Introduction

In different parts of the world, it is possible to encounter stone bridges that are worthy of the historical heritage of the day. These bridges are on the active trade routes during the period of building, but today they are becoming more important with their historical values. Protecting these monuments' original features and preserving them safely for the future is only possible by carrying out protection and repair operations. Determination of the behavior of these bridges increases the effectiveness of current and repair operations.
Bridges are one of the most important elements of the transportation infrastructure systems of many countries. Historical bridges are still being used in many different places. In Europe, 60% of railways and culverts consist of historic arch bridges. According to recent research, the number of historical arch bridges used in railways in Europe is around 200,000 [1].

In Turkey, the number of active bridges increased from 5168 to 8030 between 2002 and 2017. The number of stone bridges, which are actively used, decreased from 120 to 15 between 2002 and 2017. The reason for this decline is that the historical bridges go out of the road network and they are decided to be preserved as cultural assets, etc. [2]. There are 1816 historical bridges in Turkey. 77.92% of these bridges were built in the Ottoman, 8.82% in Seljuk, 7.48% in Rome, 1.32% in Eastern Rome, and 4.46% in the Republican periods. 94.77% of these bridges are stone arc bridges [3]. A typical arch bridge and definitions used for these bridges are shown in Fig. 1. Some elements or materials are ignored depending on the architectural age or location of the bridge [4].

* Corresponding author (irfan.kocaman@erzurum.edu.tr)

eISSN 2630-5763

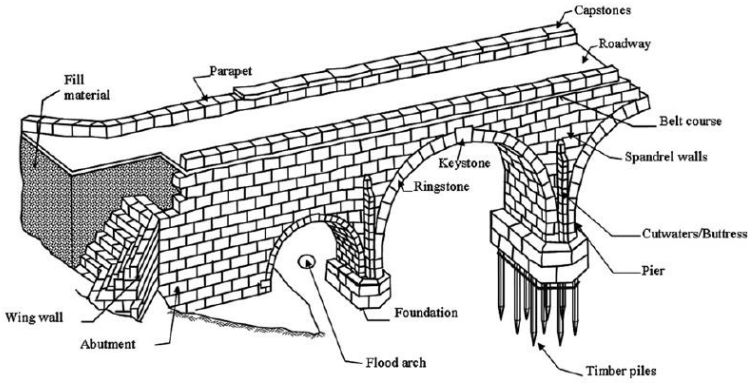

Fig. 1. Definitions used to stone arch bridges [4]

Flood and earthquake-imposed overloads are very hazardous when historical stone bridges are damaged. Because of the earthquakes and floods, stone bridges are exposed to horizontal loads, and cracks or rocking can occur on the side walls due to out-of-plane movements. Another important effect of floods is water erosion on the bridge piers. As a result of carving, cracks occur in the mortar, and the integrity between the bridge-bearing elements decays [5, 6].

Different researchers have examined the effect of lateral loads on historical bridges in the literature. Proske and Hübl [7] investigated the effect of an earthquake, flood, debris flow, damage to the bridge column or arches of ships, and the damage of these loads to historical bridges.

As mentioned above, among the reasons that may affect the safety of bridges, the effect of flood events has not received enough attention from researchers, especially in Turkey. According to studies conducted in the United States, the statistical analysis estimates that 52% of bridge collapses are due to hydraulic causes (e.g. flooding and scouring) [8]. Various factors such as climate change, urbanization, anthropogenic actions, repositioning of metering stations, or volcanic eruptions can cause an increase in flood frequency and intensity [9]. This increase is expected to adversely affect the safety of historic bridges as well as loss of life, property damage, destruction of infrastructure, and social and economic disruption.

Flood events can damage bridges in so many ways such as overtopping, accelerated scour, debris flows impact, erosion of bridge approaches, and collapse due to horizontal direct water pressure [10]. Among bridge failure studies in the world, Ratzinger and Proske [11] investigated the behavior of different elements of bridges (belt, spandrel walls, pavement, foundation, etc.) under the effect of flood events. They tried to estimate how historical stone bridges would behave under lateral load. Park et al. [12] carried out different experiments to estimate the effects of debris accumulation on the bridge pier scour. They concluded that the scour depth increased with the flow intensity. Rahimi et al. [13] studied the effect of the flow and scour pattern near bridge piers with different configurations. They proposed some modifications to the common empirical formula used for the prediction of scour depth.

In this study, the effect of horizontal direct water pressure load on the historical Çobandede bridge is discussed under different flood scenarios. Historical flood records generally are not enough to precisely estimate large floods which may cause damages. This encourages researchers to use efficient and robust statistical techniques to develop the best possible flood risk estimates about the processes involved. There are many statistical models (such as probability distributions) that are found useful. The main problem for hydrologists is to define the best distribution model for the considered time series, as there is no commonly used unique distribution for modeling extreme flood events. To define the best model that provides more accurate flood estimates, it is necessary to evaluate a sufficient number of distributions. There has been a

number of probability distributions used for modeling flood events. [14-17]. The choice of a probability distribution is an important factor in flood frequency analysis because a wrong choice can cause serious errors in the design of flood estimates, especially at higher return periods.

In this context, the research methodology can be summarized as follows. First, eleven probability distributions, namely Gamma (GAM), Generalized Extreme Value (GEV), Exponential (EXP), Gumbel (GUM), Log-Logistic (LLOGIS), Logistic (LOGIS), two parameters Lognormal (LN2), three parameters Lognormal (LN2) Normal (NORM), Pearson type-III, and Weibull (WBL), are used for modeling flood records. Second, the Maximum likelihood method (MLM) is used to estimate the parameters of the considered distributions. The most suitable probability distributions are evaluated using Kolmogorov-Smirnov (KS), Cramér-von-Mises (CvM), Anderson Darling (AD), and two information-based criteria including Akaike Information Criteria (AIC) and Bayesian Information Criteria (BIC) tests. Using selected best-fit models, T-year floods (20, 50, 100, 200, 500, and 1000) are estimated. Third, the velocities corresponding to the calculated flow data are calculated with the Manning-Strickler Formula. Finally, the finite element model of Çobandede Bridge that is created in ANSYS APDL software is analyzed under flood loads. The determined maximum speed value has been converted to the pressure value by the method suggested in ASSHO [18]. The behavior of the bridge is examined under flood pressure forces.

2. Çobandede bridge

2.1. General features

Historical Çobandede Bridge is located in the Erzurum-Kars section of the Eastern Anatolia Region, one kilometer east of the Köprüköy district center. The bridge is located in the narrowest area in the east of the Pasinler Plain (at 1555 m altitude). The bridge is also located on the south of Çobandede Mountain, on the Aras River which is formed by the combination of the Hasankale (Kargapazarı) and Bingöl Rivers (Fig. 2) [19].

The bridge was built in 1297-1298 by Emir Çoban Salduz grand vizier of the Ilhanlı ruler Gazan Han. The bridge was built in the form of a bow to provide a steep encounter with rivers from two different directions. The placement of foundations on wooden piles flattened and pointed arches, resting cells (little room) on each foot, and the ornaments in the temples and heels represent the architectural character of the period [20].

Fig. 2. Upper reach view Çobandede bridge

The length of the bridge is 220 m. In total, it consists of 7 spans. The largest arch span is 16.8 m and the height of the keystone is 14.2 m. During the repairs carried out on the bridge in previous years, the arch at the northern end of the bridge was filled. Currently, the closed arch was reconstructed in its original form during the repair made in 2013. The restoration of the bridge was completed in 2014 by the General Directorate of Highways [20].

2.2. Finite element model

The development of the finite elemental models of historical structures is difficult due to different load-bearing systems and detailed architectural features. However, with today's technology, developing software and computers made it possible to model complex baths, bridges, mosques, and many other masonry structures. The finite element model of Çobandede Bridge is created in ANSYS software [21]. The finite element model is composed of 52,122 nodes and 64,444 elements as shown in Fig. 3. While the finite element model is being created, geometrical properties of the structure are obtained by in situ studies.

The SOLID65 element is used in the finite element models, and the five-parameter Willam-Warnke [22] model developed for concrete and geomaterials is used as the material model. In the Willam-Wranke model, the failure surface of the material is created by using the tensile and compressive strengths of the stone or masonry unit. If the material at an integration point fails in uniaxial, biaxial, or triaxial compression, the material is assumed to crush at that point. In SOLID65, crushing is defined as the complete deterioration of the structural integrity of the material (e.g. material spalling). Under conditions where crushing has occurred, material strength is assumed to have degraded to an extent such that the contribution to the stiffness of an element at the integration point in question can be ignored. Although both the SOLID65 element and the Willam-Wranke material model were originally developed to describe the behavior of concrete, they are also widely used in masonry with the correct definition of the main parameters [23-26]. The parameters used to define the failure surface in the material model are the crushing strength (f_c), tensile strength (f_t), and shear transfer coefficients for open (β_t) and closed (β_c) cracks. In the analysis, β_t value is defined as 0.8, and β_c value is defined as 0.05 [23, 24].

2.3. Material properties

It is difficult to determine the material properties in historical structures as in these old and large-scale structures the mechanical properties of the materials are not homogeneous and it is not always possible to take a sample from the structure to determine the mechanical properties of the materials. For this reason, the material properties of the Çobandede Bridge are determined using available literature.

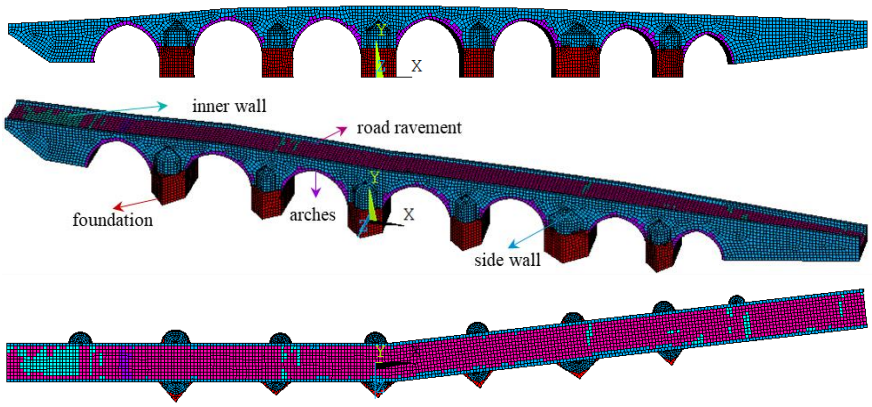

Fig. 3. The finite element model of the Çobandede bridge

Table 1. Material properties used in the finite element model

	Elasticity modulus (MPa)	Poisson ratio	Density (t/m^3)
Arches	3000	0.25	2.45
Side Wall	2500	0.18	2.35
Inner Wall	2000	0.05	1.25
Foundation	6000	0.25	2.45
Road Pavement	1500	0.10	1.25

Ural et al. [4] determined the elastic modulus as 3000, 2800, 2500, 1500, and 6000 MPa respectively in arches, outer walls, road pavement, inner walls (filler), and foundations of the historical Değirmendere Bridge. Bayraktar et al. [27] obtained the material properties of the Şenyuva Bridge by calibrating experimental and theoretical modal analysis results. According to measurements, the elastic modulus of 3000, 1500, and 2500 MPa, Poisson's ratio of 0.25, 0.05, and 0.20, and density of 1600, 1300, and 1400 kg/m^3 are identified at the outer walls, the road pavement, and the inner and side wall parts, respectively. The material properties employed in the finite element model of the Çobandede Bridge are given in Table 1.

2.4. Modal analysis

Mode shapes and modal periods of Çobandede Bridge are obtained by modal analysis. Modal analysis is done for the first twenty modes and the first three modes have been focused on. In Table 2, frequencies and mass participation factors of the first three modes are given. Mode shapes are given in Fig. 4. The total mass of the bridge is calculated as 29,230 tons.

In regards to mode shapes, the 1st mode is in the transverse direction (*z*-direction), the 2nd mode is in the longitudinal direction (*x*-direction) and the 3rd mode is in the second transverse mode. When the deformations in each mode shape are investigated, it is predicted that during an earthquake the stresses will be concentrated in the arches and connection area between the arches and the bridge piers.

2.5. Gravity analysis

Static analysis of the bridge is carried out under the gravity load. According to the analysis, maximum displacements (vertical direction) occur in keystone areas of arches. These displacements are 2.62 mm, 2.4 mm, and 2.4 mm in the 2nd, 3^{rd,} and 4th arches, respectively (Fig. 5).

Upon investigation of the compressive and tensile stresses, it is seen that compressive stresses are concentrated at the foundations and connection areas between arches and columns. The maximum compressive stress is observed as 1.19 MPa as plotted in Fig. 6(a). The tensile stresses are concentrated at keystones of the arches, curved road pavement, and cupola of cutwaters. The maximum tensile stress is observed as 0.06 MPa as displayed in Fig. 6(b). However, local stresses in the stone walls on the sides of the road reach levels of 0.19 MPa. Maximum tensile and compressive strength values are less than the values accepted in material properties (0.3 MPa for tensile, 7.29 MPa for compressive). Stresses are below the typical stress limits that may occur under static loading situations at the bridges.

2.6. Pushover analysis

Static pushover analysis is a simple yet effective method for the determination of the lateral force capacity of structures. The nonlinear force-displacement relationship of structures can be determined using a lateral load pattern mimicking the modal force distribution of the mode with the largest mass participation ratio under the assumption that the dynamic behavior is dominated by this mode. However, it should not be correct to calculate the generalized lateral load-displacement curves of long-span multi-arch masonry bridges using

the total span of the bridge, especially in the transverse direction. The low modal mass participation ratios in both directions and Mode 1 shape in Fig. 4 indicate that only the laterally most flexible middle span arches contribute most of the modal force (the modal mass participation ratio of 0.205 mostly consists of this part's mass). Özkaya [28] demonstrated that for single-span arch bridges a pushover curve calculated by applying a uniform load on the lateral surface of the arch and spandrel walls covering the length of the arch span and additional zones on the edges agrees well with the load-deformation response over the same region under seismic excitation.

Table 2. Frequencies and mass participation factors of the first three modes of the Çobandede Bridge

Mode	Frequency (Hz)	Mass Part. Fac. (*x*, longitudinal)	Mass Part. Fac. (*y*, vertical)	Mass Part. Fac. (*z*, transverse)	Mass Part. Fac. (*y*, rotation)
1	6.38	0.225E-02	0.265E-04	0.203	0.917E-03
2	6.73	0.345	0.231E-04	0.190E-02	0.114E-02
3	6.91	0.405E-02	0.438E-06	0.245E-02	0.576E-01

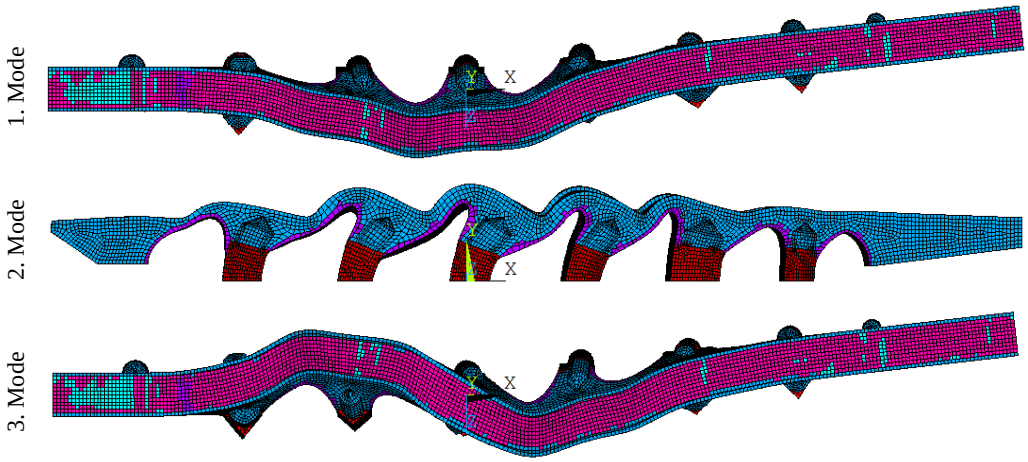

Fig. 4. Deformation patterns of the first three modes of Çobandede Bridge

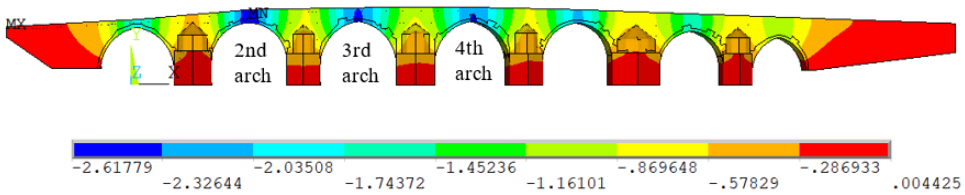

Fig. 5. Vertical displacements under gravity load (mm)

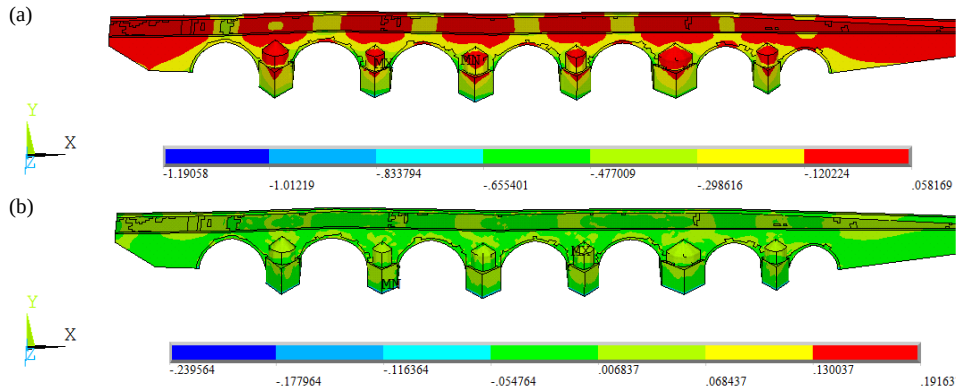

Fig. 6. (a) Compressive stresses, (b) tensile stresses under gravity load (MPa)

The lateral capacity of masonry structures can be found correctly with uniformly distributed acceleration loading [23, 24]. The lateral force-displacement curves for the 2nd, 3rd, and 4th arches that are calculated under uniformly distributed acceleration loading along the height are given in Fig. 7. Along with the reasons given above, the force values for each arch are calculated from the elements along the periphery of bounding boxes shown in Fig. 8. Here, the displacements are taken on the keystone of each arch. Due to their similarity, each arch has a similar load-deformation capacity. Since local lateral strength is assumed to determine the behavior of the bridge under lateral loads, it would be reasonable to evaluate the lateral strength of the bridge in terms of the strength to be provided by the spans and adjacent bridge piers.

About Fig. 7, it is seen that the transverse-lateral load capacity of each arch is approximately 12,000 kN. The principal strain distribution at the maximum force is given in Fig. 8. When the bridge reaches transverse-lateral force capacity, the strain value is approximately 0.003.

3. Statistical model for floods: Use of probability distributions

In the present study, eleven popular probability distributions, namely Gamma (GAM), Generalized Extreme Value (GEV), Exponential (EXP), Gumbel (GUM), Log-Logistic (LLOGIS), Logistic (LOGIS), two parameters Lognormal (LN2), three parameters Lognormal (LN2) Normal (NORM), Pearson type-III, and Weibull (WBL), were applied for modeling flood records. The probability density functions (PDF) of these distributions and their related parameters are presented in Table 3. Parameters of the considered distributions are estimated using the Maximum Likelihood Method (MLM) which is briefly described in the following section.

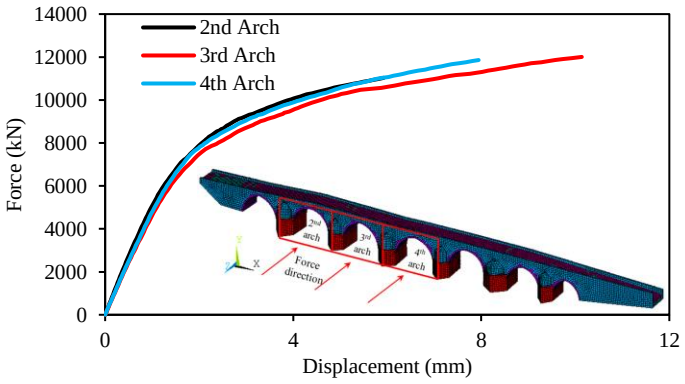

Fig. 7. Force-displacement relation of the 2nd, 3rd and 4th arches in the transverse direction

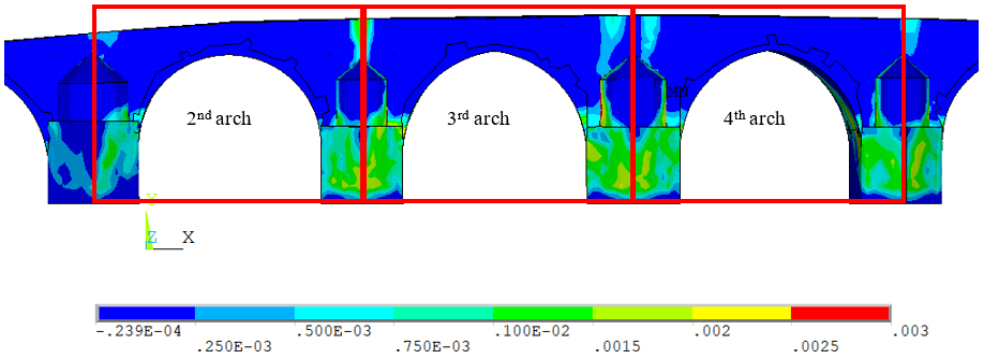

Fig. 8. 1st principal strain distribution obtained from pushover analysis

3.1. Maximum likelihood method (MLM)

MLM is the most effective parameter estimation method, especially for large flow sample sizes [29]. In this method, the parameters of a probability distribution are estimated by maximizing the log-likelihood function. Supposing that there are m independent and identically distributed observations $x_1, x_2, \ldots, x_m$. Then, the log-likelihood function $x_1, x_2, \ldots, x_m$ is defined as the joint probability of $\varepsilon_1, \ldots\ldots, \varepsilon_N$ (errors for different points in the data), and this function is derived from

$$L(\varepsilon) = \prod_{i=1}^{n} f(\varepsilon_i, x_1, x_2, \ldots\ldots\ldots x_m) \quad (1)$$

where $f(x_1, x_2, \ldots\ldots\ldots x_m)$ represents the probability distribution function of the data. The maximum likelihood is estimated by maximizing the function $L(\varepsilon)$ for given data x.

3.2. Definition of the best model: Model selection criteria/techniques

In this study, five commonly used goodness of fit tests, namely Kolmogorov-Smirnov (KS), Cramér-von-Mises (CvM), Anderson Darling (AD), and two information-based criteria including Akaike Information Criteria (AIC) and Bayesian Information Criteria (BIC) are used to define the most appropriate probability distribution function for the time series.

3.2.1. Kolmogorov-Smirnov test (KS)

KS test is a goodness of fit statistic that compares the empirical cumulative distribution function (F_x) with the theoretical cumulative distribution function (F_y) of reference distribution based on the distance. KS statistic can be calculated as follows:

$$D = max\left|F_x(x) - F_y(y)\right| \quad (2)$$

The rationale behind the KS test is simply based on the maximum absolute vertical distance between determined and observed cumulative distribution functions. The Calculated D value is compared with the Kolmogorov-Smirnov table of critical values to reject or accept the null hypothesis at desired significance level. If the calculated D statistic is less than the critical value read from the KS table at the α significance level ($D_{table} > D$), it results that the chosen probability distribution is the suitable distribution for the data.

3.2.2. Cramér-von Mises test (CvM)

Similar to the KS test, the CvM relies on the comparison of empirical and theoretical cumulative distribution functions. The CvM statistic, W^2, is computed with the following formula [30]:

$$W^2 = \frac{1}{12n} + \sum_{i=1}^{n}\left[F(x_i) - \frac{2i-1}{2n}\right]^2 \quad (3)$$

where n is the length of the data number, x_i represents the ith order statistic of the sample x_1, x_2, x_3…… x_n which is sorted from smallest to largest. If the test statistic, W^2, is smaller than the critical table value, the data is considered to follow the specified distribution.

3.2.3. Anderson Darling test (AD)

The AD test is similar to the KS test. It is more sensitive than the CvM to data in the tail of a distribution, thus it is more effective in determining outliers [30]. The test statistic of the AD, A^2, is computed as follows:

$$A^2 = -n - \frac{1}{n}\sum_{i=1}^{n}(2i-1)\{ln\,F(x_i) + ln\,[1 - F(x_{n-i+1})]\} \quad (4)$$

where $F(x_i)$ represents the cumulative distribution function of the tested theoretical distribution. The AD test statistic, A^2, is compared with the critical table value that depends on the determined PDF, to decide whether to accept or reject the null hypothesis. If the A^2 statistic is greater than the AD critical table value at a certain significance level, the null hypothesis that sample data follows the determined PDF is rejected. Among the different probability distributions found suitable, the best type is the one with the minimum test (KS, CvM, and AD) value.

3.2.4. Akaike information criterion (AIC)

The AIC provides a comparative assessment of the suitability of various models to a particular dataset. In this criterion presented by Akaike [31], the most appropriate model is one with a minimum AIC value. The AIC value is computed with the following formula:

$$\mathrm{AIC} = -2L + 2p \quad (5)$$

where L is the maximum log-likelihood value of the probability distribution model that fits the data and. p is the number of predictable model parameters that fit the sample data.

3.2.5. Bayesian information criterion (BIC)

The BIC suggested by Schwarz [32] is utilized to determine the most appropriate model. Similar to AIC, the smallest BIC value refers to the best model for a given dataset. The BIC value is computed with the following formula:

$$\mathrm{BIC} = -2\,log\,L + p log(n) \quad (6)$$

where L represents the maximum value of the log-likelihood under the fitted model, p is the number of parameters in the corresponding distribution and n is the sample size.

4. Flood data and study area

The Aras River Basin, which is located in the eastern Anatolia region of Turkey, is one of the major and important hydrological basins of Turkey. The river springs from Bingöl Mountains and reaches Nakhichevan after a course of 548 km. In the region, winters are long, cold, and relatively dry, springs are cool and wet while dry weather conditions are seen in summer. The annual mean temperature is 10.2 °C and the mean of total annual precipitation is 579.4 mm [33]. Kağızman Basin, a subbasin of the Aras River, is selected as a study for application as shown in Fig. 9. The basin is the drainage area of flow gauging station 2402

controlled by the General Directorate of State Hydraulic Works in Turkey. Aşağı Kağdariç Basin has an area of 8872.8 km^2.

In this study, annual instantaneous maximum flows (AIMF) from a gauge station, which is located at the source of the bridge, were considered for statistical modeling. The main reason for choosing this station is that the observations are not affected by human intervention, they show homogeneity and there is no missing value. The AIMF data, which has a record length of 30 years, was obtained from the General Directorate of State Hydraulic Works, Turkey. Major statistical characteristics of the AIMF series are presented in Table 3.

5. Results

5.1. Selection of the best probability distributions for the AIMF series

Before applying models (probability distributions) to the AIMF series, the independence and stationarity of the data series, which are necessary assumptions in conventional frequency analysis, should be checked [34, 35]. To this end, we used the nonparametric Mann-Kendall trend [10, 36] and the Ljung-Box [37] tests to analyze the stationarity and serial autocorrelation of the data. Results of the both tests are also presented in Table 4. As can be seen from the table, there was no significant trend and autocorrelation as the computed *p* values were larger than 0.05.

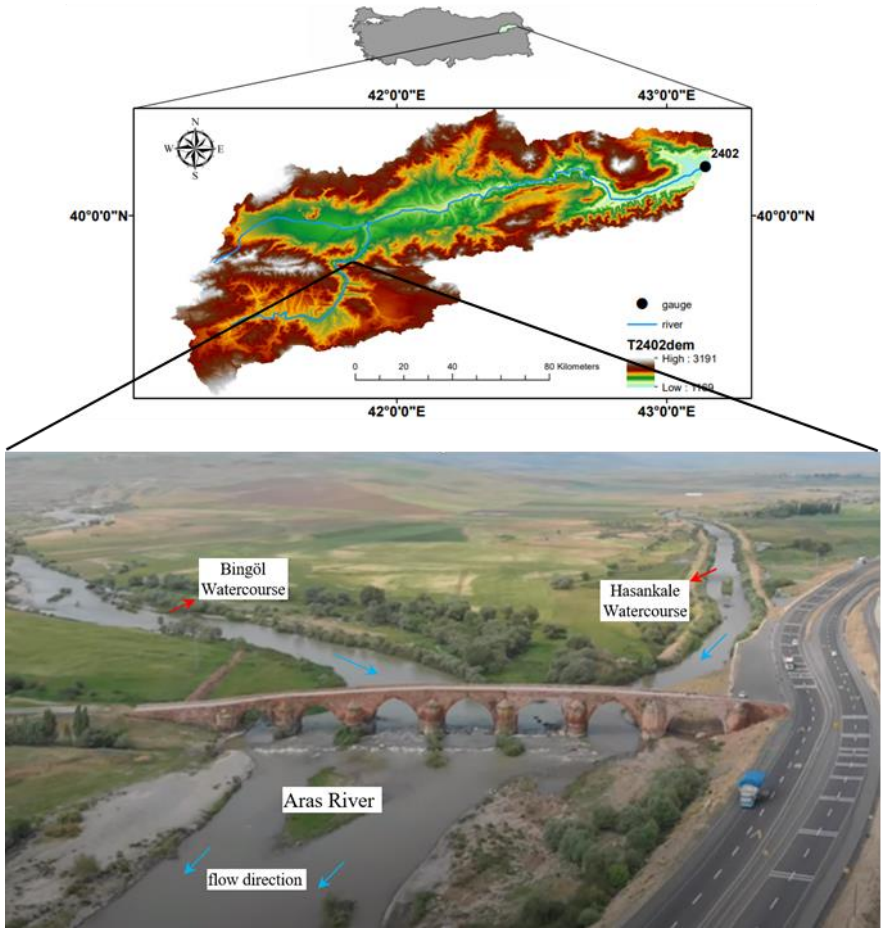

Fig. 9. Study area and Çobandede bridge drone image

Table 3. General description of the probability distribution functions considered in the study

Distribution Type	Probability Distribution Function	Parameters
Weibull (WBL)	$f(x) = \frac{k}{\alpha}\left(\frac{x}{\alpha}\right)^{k-1} exp\left[-\left(\frac{x}{\alpha}\right)^{k}\right]$	k: shape parameter (k>0) α: scale parameter (α>0)
Two Parameter Lognormal (LNORM)	$f(x) = \frac{1}{x\sigma_y\sqrt{2\pi}} exp\left[-\frac{1}{2{\sigma_y}^2}\left(logx - \mu_y\right)^2\right]$	μ_y: shape parameter (μ_y>0) σ_y: scale parameter (σ_y>0) t: threshold parameter
Three Parameter Lognormal (LNORM3)	$f(x) = \frac{1}{(x-t)\sigma_y\sqrt{2\pi}} exp\left[-\frac{1}{2{\sigma_y}^2}\left(\log(x-t) - \mu_y\right)^2\right]$	
Gamma (G2)	$f(x) = \frac{x^{k-1}}{\alpha^k \Gamma(k)} exp\left[\frac{-(x)}{\alpha}\right]$	k: shape parameter (k>0) α: scale parameter (α>0) t: threshold parameter Γ: gamma function
Pearson Type III (P3)	$f(x) = \frac{(x-t)^{k-1}}{\alpha^k \Gamma(k)} exp\left[\frac{-(x-t)}{\alpha}\right]$	
Normal (NORM)	$f(x) = \frac{1}{\sigma\sqrt{2\pi}} exp\left[\frac{-1}{2}\left(\frac{x-\mu}{\sigma}\right)^2\right]$	μ: mean (location parameter) σ: standard deviation (scale parameter) (σ>0)
Gumbel (EV1)	$f(x) = \frac{1}{\sigma} exp\left[-\frac{(x-\mu)}{\sigma} - exp\left(-\frac{(x-\mu)}{\sigma}\right)\right]$	μ: mean (location parameter) σ: standard deviation (scale parameter) (σ>0)
Logistic (LOGIS)	$f(x) = \frac{1}{\alpha}\exp\left(\frac{x-\xi}{\alpha}\right)\left[1 + \exp\left(\frac{x-\xi}{\alpha}\right)\right]^{-2}$	ξ: location parameter α: scale parameter (α>0) k: shape parameter
Log-logistic (LLOGIS)	$f(x) = \frac{k}{x}\left(\frac{x}{\alpha}\right)^{k}\left[1 + \left(\frac{x}{\alpha}\right)^{k}\right]^{-2}$	
Generalized Extreme Value (GEV)	$f(x) = \frac{1}{\alpha}\exp\left[-(1+kz)^{-1/k}\right](1+kz)^{-1-1/k}$	ξ: location parameter α: scale parameter (α>0) k: shape parameter $\left(z = \frac{x-\xi}{\alpha}\right)$

Table 4. Results of Mann-Kendall and Ljung-Box tests

	Mann-Kendall Test			Ljung-Box Test	
AGI	Test Statistic (S)	Z value	*p*-value	Test Statistic (Q)	*p*-value
2402	-29	-0.450	0.617	16.794	0.666

Gamma (GAM), Generalized Extreme Value (GEV), Exponential (EXP), Gumbel (GUM), Log-Logistic (LLOGIS), Logistic (LOGIS), two parameters Lognormal (LN2), three parameters Lognormal (LN2), Normal (NORM), Pearson type-III (PEAR3), and Weibull (WBL) were used to model the AIMF series. Performances of the fitted distributions were compared by the Akaike Information Criterion (AIC), the Anderson-Darling Criterion (ADC), the Bayesian information criterion (BIC), the Cramér-von-Mises test (CvM), and the Kolmogorov–Smirnov (KS) tests and the results are given in Table 4. It is obvious from the table that the LLOGIS distribution, which provides the lowest value for all tests, was found to be the most suitable one for modeling the AIMF series. For visual assessment, the probability density function (PDF), cumulative distribution function (CDF), Probability-Probability (P-P), and Quantile-Quantile (Q-Q) plots of the LLOGIS against the empirical distributions were drawn (Fig. 10). It can be seen from these plots that the selected LLOGIS distribution provided a good agreement with empirical data.

Once the best-fitted distribution has been defined and validated, it can be employed to estimate the quantile corresponding to a given return period or, conversely, to compute the return period of specified events. The univariate return periods for the AIMF series can be computed as

$$T = \frac{\mu}{1 - F_Q(q)} \tag{7}$$

where μ is the expected flood inter-arrival time and it is equal to 1 if annual maximum variables are considered. $F_Q(q)$ denotes the CDF of the AIMF series. The quantile AIMF values for any return period can be also estimated using this formula. In this study, the AIMF values that have return periods of 20, 50, 100, 200, 500, and 1000 years were computed. Then, the corresponding velocities were computed in Table 5 by using Manning-Strickler Formula as

$$V = \frac{1}{n} \cdot R^{2/3} \cdot J_0^{1/2} \tag{7}$$

where R is hydraulic radius, n is coefficient of roughness and J_0 denotes channel bottom slope.

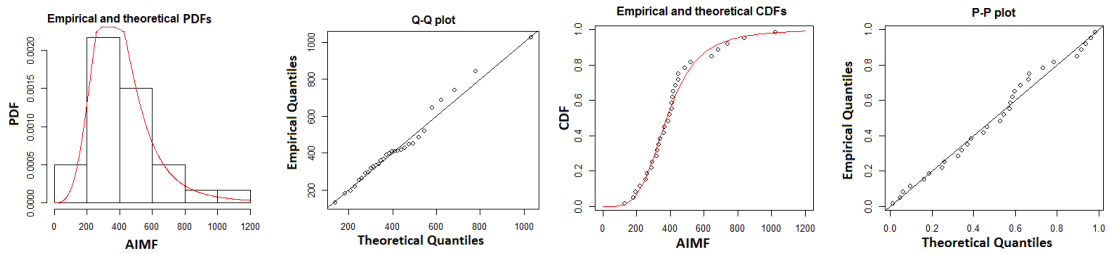

Fig. 10. PDF, CDF, P-P, and Q-Q plot representations of the best-fitted univariate distributions for the AIMF series

Table 5. AIMF, *H*, *R*, and *V* values in different return periods

Return period (*T*) (years)	The estimated AIMF (m^3/s)	*H* (m)	*R* (m)	*V* (m/s)
20	781	1.398	1.350	3.701
50	986	1.974	1.881	3.265
100	1172	2.871	2.682	4.136
200	1392	3.178	2.949	4.406
500	1745	3.632	3.338	4.786
1000	2069	2.496	2.351	5.357

5.2. The behavior of Çobandede Bridge under flood load

The Çobandede Bridge is located in a region where two different rivers join as shown in Fig 9. The bridge originally was built perpendicular to the flow direction just below the junction of the two tributaries of the river. However, the change of streambed over time has caused these two rivers to stay no longer perpendicular to the bridge. For this reason, lateral water pressures have also begun to affect the bridge besides vertical water pressure. As seen in Fig. 9, the Hasankale tributary has an approach angle of 25° from the north part of the bridge and the Bingöl tributary has an angle of 20° from the southern part of the bridge. Using this information, the pressure load on the bridge foundation is [18]

$$p = 800 \times C_d \times V^2 \tag{9}$$

where p is the pressure of the flowing water in Pa, V is the design velocity of water for the design flood in strength and service limit states, and a check flood in the extreme event limit state (m/s), C_D is the drag coefficient for piers. The drag coefficient is determined by the geometry of cutwaters (buttress). The geometry of the cutwaters of Çobandede Bridge is a triangle. So the drag coefficient (C_D) is taken at 0.8.

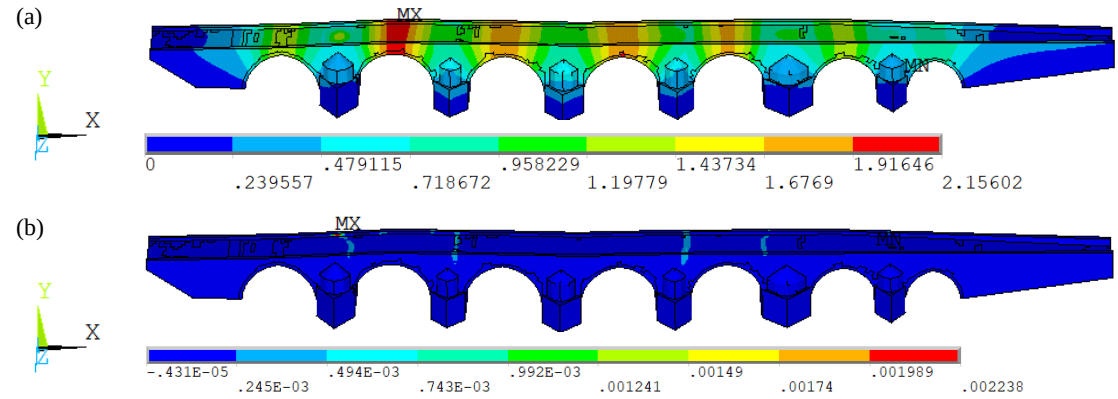

Fig. 11. Under flood load (a) transverse displacements (b) 1st principal strain distributions

When the bridge piles are exposed to water by an angle θ in the lateral direction, the pressure load is [18]

$$p = 800 \times C_L \times V^2 \tag{10}$$

where C_L is the lateral drag coefficient. This coefficient depends on the angle θ. C_L coefficient is determined to be 0.9.

Using the determined flood height and velocity values, the pressure load to be applied on the bridge columns was determined with Eq. 11. Here, the velocity value is taken from Table 5 as 4.786 (m/s) for a return period of 500 years. Although the velocity value is higher for a return period of 1000 years, these values have not been used due to the low water height (2.496 m). The pressure force which is 695 kN was loaded on the bridge statically. As shown in Fig.7, the lateral force capacity of the arches was determined approximately 12,000 kN. The flood load can't cause any damage to the bridge. However, analysis was carried out under flood load.

As a result of the analysis, maximum compressive stress and tensile stress were determined as 1.03 MPa and 0.02 MPa, respectively. The transverse displacement of the bridge (z-direction) is given in Fig. 11(a). Its maximum value is 2.15 mm on top of the arch. According to this value, the drift ratio is %0.016. These values are very low. The strain distribution is plotted in Fig. 11(b). Strains are concentered in the junction area of arches, however, the values are very low.

The results of the static analysis under flood loads show that the bridge is not affected under a flood with a return period of 500 years. The reason for this can be explained by

a) the riverbed is quite large with no obstacle to spread,
b) the cutwaters of the bridge were well-designed, and
c) the piers are very high and wide (7 m and 8.8 m respectively).

6. Conclusion

This paper provides a probabilistic framework for the risk assessment of bridges under various flood events. For this purpose, the behavior of historical bridges under the maximum possible water loading has been examined. The finite element model of the historical Çobandede bridge was created with ANSYS software. The flood load that could come onto the bridge was determined by examining different statistical methods. Static analysis was performed by applying the determined water load on the bridge. As a result of the analysis, the historical bridge is not expected to be damaged in light of the water velocity calculated in return periods of 20, 50, 100, 200, 500, and 1000 years.

This study is important to draw attention to a different problem as historical bridges are important in terms of cultural heritage and transportation networks. Changing climatic conditions, irregular and heavy rainfall, etc. can cause damage to historic bridges by water loads. Risk analysis of historical bridges under water loads will be an important step to find solutions to climatic problems that may occur in the near future. Furthermore, we hope that the analysis methods presented in this study can produce important knowledge and foresight for engineers on the design of structures to be constructed within the watershed covered by the study area.

Declaration of conflicting interests

The author(s) declared no potential conflicts of interest with respect to the research, authorship, and/or publication of this article.

References

[1] International Union of Railways: Improving Assessment, Optimization of Maintenance and Development of Database for Masonry Arch Bridges. http://orisoft.pmmf.hu/masonry/. Accessed 26 April 2018.

[2] Republic of Turkey General Directorate of Highways: Bridges inventory data. http://www.kgm.gov.tr. Accessed 26 April 2018.

[3] Republic of Turkey General Directorate of National Roads and Buildings: Department of Arts. http://www.kgm.gov.tr. Accessed 26 April 2018.

[4] Ural A, Oruc S, Dogangun A, Tuluk OI (2008) Turkish historical arch bridges and their deteriorations and failures. Engineering Failure Analysis 15:43-53.

[5] Türker T (2014) Structural evaluation of Aspendos (Belkıs) masonry bridge. Structural Engineering and Mechanics 50(4):419-439.

[6] Liao KW, Hoang ND, Gitomarsono JA (2018) Probabilistic safety evaluation framework for multi-hazard assessment in a bridge using SO-MARS learning model. KSCE Journal of Civil Engineering 22:903-915.

[7] Proske D, Hübl J (2007) Historical arch bridges under horizontal loads. In: 5th International Conference on Arch Bridges. Madeira, Portugal.

[8] Cook W, Barr PJ, Halling MW (2015) Bridge failure rate. Journal of Performance of Constructed Facilities-ASCE 29(3). https://doi.org/10.1061/(ASCE)CF.1943-5509.0000571.

[9] Yue S, Kundzewicz ZW, Wang L (2012) Changes in Flood Risk in Europe. CRC Press and IAHS Press, Wallingford, UK, pp. 387-408.

[10] Kendall MG (1975) Rank Correlation Methods. Charless Griffin, London.

[11] Ratzinger K, Proske D (2010) Historical stone arch bridges under horizontal debris flow impact. In: 6th International Conference on Arch Bridges. Fuzhou, China.

[12] Park JH, Sok C, Park CK, Kim YD (2016) A study on the effects of debris accumulation at sacrificial piles on bridge pier scour: I. Experimental results. KSCE Journal of Civil Engineering 20(4):1546-1551.

[13] Rahimi E, Qaderi K, Rahimpour M, Ahmadi MM (2018) Effect of debris on piers group scour: An experimental study. KSCE Journal of Civil Engineering 22(4):1496-1505.

[14] Can I, Tosunoglu F (2013) Estimating T-year flood confidence intervals of rivers in Çoruh Basin, Turkey. Journal of Flood Risk Management 6:186-196.

[15] Anilan T, Satilmis U, Kankal M, Yuksek O (2016) Application of artificial neural networks and regression analysis to L-moments based regional frequency analysis in the Eastern Black Sea Basin, Turkey. KSCE Journal of Civil Engineering 20(5):2082-2092.

[16] Ahmadi F, Radmaneh F, Parham GA, Mirabbasi R (2017) Comparison of the performance of power law and probability distributions in the frequency analysis of flood in Dez Basin, Iran. Natural Hazards 87:1313-1331.

[17] Heidarpour B, Saghafian B, Yazdi J, Azamathulla HM (2017) Effect of extraordinary large floods on at-site flood frequency. Water Resource Management 31:4187–4205.

[18] American Association of State Highway and Transportation Officials (AASHTO). LRFD bridge design specifications (2010) Washington DC, USA.

[19] Soylu H (1997) Geographical location and importance of Çobandede Bridge. Çobandede Bridge in Our History and Culture Life Panel, Erzurum.
[20] Republic of Turkey General Directorate of Highways. 12th Regional Directorate of Highways Historical Bridges Booklet, Erzurum.
[21] ANSYS, Finite Element Analysis Program (2020) ANSYS, Inc., Southpointe, 2600 Ansys Drive, Canonsburg, PA 15317, USA.
[22] Willam KJ, Warnke ED (1975) Constitutive model for the triaxial behavior of concrete. International Association for Bridge and Structural Engineering 19(3):1-30.
[23] Kazaz İ, Kocaman İ (2018) Seismic load capacity evaluation of stone masonry mosques. Journal of the Faculty of Engineering and Architecture of Gazi University 33(2):543-558.
[24] Kocaman İ, Kazaz İ, Kazaz E (2020) Seismic load capacity of historical masonry mosques by rigid body kinetics. International Journal of Architectural Heritage 14(6):849-869.
[25] Kocaman İ, Kazaz İ, Okuyucu D (2018) Investigation of the structural behavior of the historical Erzurum Yakutiye Madrasah. Dokuz Eylul University Journal of Science and Engineering 20(58):36-51.
[26] Kazaz İ, Yakut A, Gülkan P (2006) Numerical simulation of dynamic shear wall tests: A benchmark study. Computers & Structures 84(8-9):549-562.
[27] Özkaya GS (2019) Estimation of earthquake behavior of masonry bridges with nonlinear static methods, Ph.D. Thesis, Erzurum Technical University, Erzurum.
[28] Bayraktar A, Birinci F, Altunisik AC (2009) Finite element model updating of Senyuva historical arch bridge using ambient vibration tests. Baltic Journal of Road and Bridge Engineering 4(4):177-185.
[29] Gharib A, Davies EGR, Goss GG, Faramarzi M (2017) Assessment of the combined effects of threshold selection and parameter estimation of generalized Pareto distribution with applications to flood frequency analysis. Water 9(9):692.
[30] Ashkar F, Aucoin F, Choulakian V, Vautour C (2013) Cramer-von Mises and Anderson-Darling goodness-of-fit tests for the two-parameter kappa distribution. Hydrological Sciences Journal 62(7):1167-1180.
[31] Akaike H (1974) A new look at the statistical model identification. IEEE Transactions on Automatic Control 19(6).
[32] Schwarz G (1978) Estimating the dimension of a model. The Analysis of Statistics 6:461-464.
[33] Karaoglu M (2014). Agricultural meteorological properties of Aras Basin in Turkey. Turkish Journal of Agricultural Research 1:1-8.
[34] Daneshkhah A, Parham G, Chatrabgoun O, Jokar M (2016) Approximation multi-variate distribution with pair copula using the orthonormal polynomial and Legendre multi-wavelets basis functions. Communications in Statistics-Simulation and Computation 45(2):389-419.
[35] Tosunoglu F, Singh V (2018) Multivariate modeling of annual instantaneous maximum flows using copulas. Journal of Hydrologic Engineering 23(3).
[36] Mann HB (1945) Nonparametric tests against trend. Econometrica 13(3):245-259.
[37] Ljung GM, Box GEP (1978) On a measure of a lack of fit in time series Models. Biometrika 65(2):297-303.